Fermi National Accelerator Laboratory

FERMILAB-Pub-94/357-A

Analysis of Small and Medium-Scale Cosmic Microwave Background Measurements*

Scott Dodelson†

NASA/Fermilab Astrophysics Center, Fermi National Accelerator Laboratory, Batavia, IL 60510-0500

Arthur Kosowsky‡

Department of Physics, Enrico Fermi Institute, The University of Chicago, Chicago, IL 60637-1433.

(October, 1994)

Abstract

Anisotropies in the temperature of the cosmic microwave background have been detected on a range of scales by several different experiments. In principle, the largest barrier to a clean interpretation of the experimental results is contamination by foreground sources. We address this issue by projecting out likely sources of foreground contamination from seven separate small-angle and medium-angle experiments. All of the experiments are so far consistent

---

*to be published in *Physical Review Letters*

†dodelson@virgo.fnal.gov

‡akosowsky@cfa.harvard.edu. Current address: Harvard-Smithsonian Center for Astrophysics, Mail Stop 51, 60 Garden St., Cambridge, MA 02138.

with the simplest inflationary models; for $n = 1$ the experiments' combined best-fit quadrupole amplitude is $Q_{\rm rms-ps} = 18^{+3}_{-1}\ \mu K$, in excellent agreement with the COBE two-year data.

98.70.Vc

More than any other cosmological observation, measurements of temperature anisotropies in the Cosmic Microwave Background (CMB) are a direct probe of the primordial spectrum of metric perturbations. Since the COBE satellite made the first anisotropy detection in 1992 [1], nearly a dozen other experiments have announced positive detections on a wide range of angular scales at amplitudes of a few parts in 10^5 of the background temperature [2]. Detector sensitivities have improved to the point where systematic errors now dominate detector noise, and the coming few rounds of experiments will increase sky coverage and reduce systematic errors. One source of error which experimental improvements cannot reduce is foreground contamination: for a given measurement, how much of the signal comes from the blackbody CMB and how much from other sources of microwave radiation?

Two different techniques are useful for sorting out the foreground. The first is to extrapolate sky maps at other frequencies (e.g. radio maps) to estimate the microwave emission in various parts of the sky, and then subtract this from the measured signal to obtain the cosmic signal. This process depends on detailed modeling of various sources and involves uncontrolled extrapolations over large frequency ranges. In this paper we focus on the complementary method of using measurements at multiple frequency channels to eliminate the non-blackbody piece of the measured signal. Clearly, as measurements improve, a combination of the two methods will give the most reliable interpretation of experiments; here we show how much various measurements may be affected by foreground contamination.

We analyze several small-scale and medium-scale anisotropy measurements which employ multiple frequencies and for which data is publicly available: MAX [3], MSAM [4], South Pole [5], and Saskatoon [6]. More current data covering larger sky fractions are now available, but the level at which foreground can be eliminated has not yet substantially improved. All measure in either three or four frequency channels. Saskatoon measures at the largest angular scale, roughly two degrees, and South Pole is slightly smaller; we call these two experiments "medium-angle." MSAM and MAX measure at smaller scales, roughly 20 to 30 arc-minutes; these are referred to as "small-angle." The angular scale is more precisely characterized by the window function W_ℓ of each experiment, defined as follows: If the sky temperature with

mean $T_0 = 2.735°$ K is decomposed into spherical harmonics as $T = T_0(1 + \sum_{\ell m} a_{\ell m} Y_{\ell m})$, then the experiment will measure a mean temperature variance (in the absence of noise) given by

$$\left(\frac{\delta T}{T_0}\right)^2 = \sum_{\ell=2}^{\infty} \frac{W_\ell}{4\pi} \sum_{m=-l}^{l} |a_{lm}|^2 . \tag{1}$$

For the purposes of the likelihood analysis presented below, the window function is extended to covariances between temperatures measured at different points on the sky. We have calculated window functions for the experiments considered here including scanning pattern on the sky, chopping strategy, and beam profiles for each frequency band.

We employ the well-known method of Bayesian likelihood analysis [7] to the data from each of these experiments, using the likelihood function

$$\mathcal{L} = \frac{(2\pi)^{-N/2}}{\sqrt{\det C}} \exp\left[-\frac{1}{2} D^T C^{-1} D\right] . \tag{2}$$

Here D is a data vector of length N; in this case, D contains values of the temperature anisotropy measured at N_p patches on the sky with N_c different channels (either at different frequencies or polarization states), such that $N_p N_c = N$. The correlation matrix C is the expectation value $\langle DD^T \rangle$ which has two separate pieces, the instrumental noise and the theoretical signal. The latter depends on the parameters in the theory being tested. Given a likelihood function depending on a theory with n parameters $\mathcal{P}$, we obtain an allowed 1σ region in $\mathcal{P}$ by the condition

$$\int_\Gamma d^n \mathcal{P} \mathcal{L}(\mathcal{P}) = 0.68; \qquad \mathcal{L}(\Gamma) \quad \text{constant}, \tag{3}$$

where the boundary surface of the allowed region is denoted by Γ. For a single parameter, the region reduces to an interval and the boundary is its endpoints.

Multiple frequency channels allow discrimination against foreground contamination [8]. In particular, for each experiment we choose one source of foreground judged most likely to be a contaminant: for MAX and MSAM dust emission, while for South Pole and Saskatoon synchrotron emission. These choices are based on the frequency ranges of the experiments:

the high frequency experiments are more likely to be sensitive to dust while the low frequency ones more sensitive to free-free and syncrotron emission. This component is then assigned a given spectral index. For example, the signal due to free-free emission is assumed to scale with frequency as $S(\nu) = S(\nu_1)(\nu/\nu_1)^{-2.1}$. If a given experiment has only two frequency channels, then the linear combination

$$\tilde{D} \equiv D(\nu_1) - (\nu_2/\nu_1)^{2.1} D(\nu_2) \tag{4}$$

is completely independent of free-free contamination. Note that if the frequencies are closely spaced, then $\tilde{D}$ approaches the difference between the data in the two channels. This difference is zero for a cosmic signal (expected to be frequency independent), so the signal to noise ratio becomes very small in the limit of closely spaced frequencies. All other factors being equal, experiments that cover a large range of frequencies are best able to distinguish cosmic signal from foreground contaminants. This advantage shows up noticably in our analysis. For N channels, we choose $N-1$ linear combinations of the data that are independent of foreground contamination from the assumed source. In principle, it is straightforward to project out multiple sources, and to fit the spectral dependences instead of fixing a likely spectral index, but the current data are not precise enough to give significant results with such analysis. Also, a non-constant prior for the foreground amplitude (if information from, say, radio maps can be reliably extrapolated) may be incorporated through a modification of Eq. (4) [8]; here we employ the most conservative analysis of a constant prior. We take spectral indices of $+1.5$ for dust [9] and -2.7 for synchrotron, although the results depend very little on the precise values chosen.

We analyze the class of theories, based on inflation, with a primordial gaussian spectrum of isentropic density perturbations $\langle(\delta\rho/\rho)^2\rangle \propto k^n$ with k the wavenumber of the perturbation. The amplitude of the fluctuations is characterized by the parameter $Q_{\rm rms-ps}$. In these models, the microwave background temperature anisotropies also depend on a variety of cosmological parameters: the Hubble constant $H_0 = 100h\,{\rm km\,sec^{-1}\,Mpc^{-1}}$, the baryon mass fraction Ω_b, the nature of the dark matter, the equivalent mass fraction in a cosmolog-

ical constant Ω_Λ, the tensor perturbation spectrum, and the redshift of reionization z_R [12]. Recent work [13] has demonstrated that to within 10% the CMB anisotropies on angular scales of a degree and larger depend only on an effective spectral index defined by

$$\tilde{n} \equiv n - 0.28\ln(1.56 - 0.56n) - 0.00036 z_R^{3/2} + 0.26\left(1 - 2h\sqrt{1-\Omega_\Lambda}\right). \qquad (5)$$

This relationship assumes the preferred nucleosynthesis relation $\Omega_b h^2 = 0.0125$ [14] and the tensor spectrum conditions $n_T = n - 1$ and $r \equiv C_2^{(T)}/C_2 \approx 7(1-n)$ given by the simplest inflation models [15]. The effects of relaxing these conditions has been explored elsewhere [16]. Thus shifting the values of the cosmological parameters $(\Omega_B, h, \Omega_\Lambda, r, \ldots)$ only moves to a different place in $(\tilde{n},\ Q_{\rm rms-ps})$ space. This "cosmic confusion," as it has been dubbed [13], means that current microwave background measurements cannot be a strong positive test for any particular set of cosmological parameters [10]. This pessimistic outlook was the conclusion of Ref. [13] and has since been often reiterated. On the other hand, this same effect produces a powerful negative test: it is easier to disprove a theory which depends on only two parameters than to disprove one which depends on many parameters.

First we calculate the one-parameter conditional likelihood for the perturbation amplitude with the effective spectral index fixed at $\tilde{n} = 1$. The best fit value and 1σ range for $Q_{\rm rms-ps}$ are plotted for each of seven data sets in Fig. 1. The x-axis shows the region in ℓ-space to which each experiment is most sensitive; the angular scale in degrees is given roughly by $200/\ell$. COBE is sensitive to large angular scales and is displayed for reference at a small value of ℓ [17].

Figure 1a plots the allowed range of $Q_{\rm rms-ps}$ neglecting the effect of foreground; Fig. 1b projects out foreground contamination as described above. For MSAM and MAX, projecting out foreground makes little difference in the error bars because these experiments cover a large range of frequencies [18]. For Saskatoon and South Pole the error bars on $Q_{\rm rms-ps}$ become much larger when foreground is projected out [8]; note especially the South Pole experiments which cover the narrow frequency range $25 - 35$ GHz. This is because the effective signal to noise ratio is small after projecting out background from a signal spanning

a narrow frequency range, as noted above. In every case, the χ^2 per degree of freedom for the most likely amplitude is reduced by projecting out foreground. While we do not claim that these experiments are actually detecting the assumed foregrounds, the changes in the error bars quantify the extent to which these experiments can be sure they are observing a cosmic signal and not foreground contamination.

The agreement between large and small scale observations for the $\tilde{n} = 1$ model is remarkably good. The combined best fit from the seven medium/small scale experiments is $Q_{\rm rms-ps} = 18^{+3}_{-1}\mu$K, in complete agreement with the COBE two-year values [17]. The 10% uncertainty on the COBE measurement is not going to get much smaller, being dominated by cosmic variance. However, cosmic variance is not yet a major factor for the smaller scale experiments; the 10% uncertainty on $Q_{\rm rms-ps}$ from these experiments will get much smaller as sky coverage increases.

For a two-parameter fit, we now allow $\tilde{n}$ to vary and find the allowed region in ($Q_{\rm rms-ps}$, $\tilde{n}$) space for the small and medium-angle experiments. At large angles, the COBE team has performed a similar analysis; we quote their results here [17]. Figure 2 shows the regions allowed at a 1σ level by COBE, the medium angle experiments and the small angle experiments after projecting out one foreground component. A large region of consistency is currently allowed. Clearly at this stage of the observations, the medium and small-angle experiments have uncertainties which are too large to make this a powerful test. In the near future the situation will improve [2]; in fact, both Saskatoon and South Pole have made new measurements with larger frequency coverage, which should substantially reduce the error bars.

Another noticeable feature of Fig. 2 is the different slopes of the allowed regions for the three different types of experiments. The large angle results are least sloped since COBE is sensitive to the lowest order multipoles, those closest to the normalization point at $\ell = 2$. A tilt in the spectrum thus has a relatively small effect on $Q_{\rm rms-ps}$. The small angle experiments are most affected by a spectral tilt, with their best fit $Q_{\rm rms-ps}$ being significantly reduced (increased) for n large (small). The variations in slope are essential

characteristics of experiments on differing angular scales, ultimately leading to a powerful test of inflationary models.

To conclude, we have analyzed small and medium scale anisotropy experiments by projecting out one foreground component. For experiments with wide frequency coverage, this procedure does not substantially increase the error bars on the parameters in a theory. The medium and small-angle experiments we have analyzed are consistent with simple inflation models normalized to COBE, with error bars comparable to COBE. The best way to test inflation at present is to measure its two free parameters ($Q_{\rm rms-ps}$, $\tilde{n}$) at different angular scales. Current medium angle data lack the frequency coverage to discriminate effectively against foreground, so the test is not yet very powerful. However, in the next three to five years, we expect improving signal-to-noise ratios and wider frequency coverage will test inflationary models in ($Q_{\rm rms-ps}$, $\tilde{n}$) space at the 10% level.

ACKNOWLEDGMENTS

We thank Stephan Meyer and Lyman Page for patient explanations of their experiments. We are also grateful to Gary Hinshaw for useful comments. This work was supported in part by the DOE (at Chicago and Fermilab) and by NASA through grant No. NAGW-2381 (at Fermilab). AK was supported in part by the NASA Graduate Student Researchers Program.

REFERENCES

[1] G.F. Smoot *et al.*, Ap. J., **396**, L1 (1992).

[2] For a recent review of some current experimental results and associated difficulties see M. White, D. Scott, and J. Silk, Ann. Rev. Astro. Astrophys. (in press); L. Page, in Proceedings of Workshop on Cosmic Background Radiation Two Years After COBE, ed. L. Krauss (World Scientific, in press 1994).

[3] This data is from two scans of MAX3: J. Gundersen *et al.*, Ap. J. **413**, L1 (1993); P. Meinhold *et al.*, Ap. J. **409**, L1 (1993).

[4] E. S. Cheng *et al.*, Ap. J. **422**, L37 (1994) used two independent chopping schemes (MSAM2 and MSAM3) to look at the same sky at two different angular scales. Their analysis (presented in the "raw" graph in Figure 1) includes the effects of dust in a slightly different way than we do.

[5] We analyze two scans taken at the South Pole in 1991: in T. Gaier *et al.*, Ap. J. **398**, L1 (1992); J. Schuster *et al.*, Ap. J. **412**, L47 (1993).

[6] Data taken in Saskatoon in 1993: E. J. Wollack *et al.*, Ap. J. **419**, L49 (1993).

[7] A. C. S. Readhead *et al.*, Ap. J. **346**, 566 (1989).

[8] S. Dodelson and A. Stebbins, Ap. J. **433**, 440 (1994).

[9] For the MAX-GUM scan we project out cold dust and for μPeg scan warm dust with frequency dependence as given in Ref. [3].

[10] Recent work, however, shows that measuring the fluctuation spectrum down to smaller angular scales can break this degeneracy. D. Spergel, private communication (1994); A. Kosowsky, M. Kamionkowski, and G. Jungman, work in progress (1995).

[11] P. J. E. Peebles and J. T. Yu, Ap. J. **162**, 815 (1970); M. L. Wilson and J. Silk, Ap. J. **243**, 14 (1981); J. R. Bond and G. Efstathiou, Ap. J. **285**, L45 (1984); N. Vittorio and

J. Silk, Ap. J. **285**, 39 (1984); N. Sugiyama and N. Gouda, Prog. Theor. Phys. **88**, 803 (1992); S. Dodelson and J.M. Jubas, Phys. Rev. Lett. **70**, 2224 (1993); R. Crittenden, *et al.*, Phys. Rev. Lett. **71**, 324 (1993).

[12] We assume $\Omega = 1$ for this analysis, as this is a generic prediction of inflation.

[13] J.R. Bond *et al.*, Phys. Rev. Lett. **72**, 13 (1994)

[14] T.P. Walker *et al.*, Ap. J. **376**, 51 (1991).

[15] R.L. Davis *et al.*, Phys. Rev. Lett. **69**, 1856 (1992).

[16] S. Dodelson, L. Knox, and E.W. Kolb, Phys. Rev. Lett. **72**, 3444 (1994) studied the effect of relaxing the conditions on the tensor perturbation spectrum, allowing the amplitude of the tensor modes to be another free parameter. Previous work varying Ω_B and h was carried out by J.R. Bond, G. Efstathiou, P. M. Lubin, and P.R. Meinhold, Phys. Rev. Lett. **66**, 2179 (1991); S. Dodelson and J.M. Jubas, Ref. [11]; K. Gorski, R. Stompor, and R. Juszkiewicz, Ap. J. **410**, L1 (1993).

[17] K.M. Górski *et al.*, Ap. J. **430**, L89 (1994); C. L. Bennett *et al.*, Ap. J., **436**, 423 (1994). See also E. F. Bunn, D. Scott, and M. White, astro-ph/9409003 (1994).

[18] In Fig. 1b, points from both the MAX GUM scan and the μPEG scan are plotted. The μPEG scan is apparently highly contaminated by dust emission and is off the scale of Fig. 1a displaying the uncorrected data. Subsequent MAX scans in different regions of the sky have confirmed the result from the GUM scan.

FIGURES

FIG. 1. The results of seven medium and small-angular scale CMB experiments, plotted as the amplitude $Q_{\rm rms-ps}$ versus angular scale in multipole number. The effective spectral index is assumed to be $\tilde{n} = 1$. The error bars represent 1σ deviations. Figure 1a shows the raw measurements; Fig. 1b shows the same measurements after a likely foreground contaminant has been projected out.

FIG. 2. Likelihood contours plotted in $(Q_{\rm rms-ps}, \tilde{n})$ space. The overlap region between small, medium, and large-angle experiments is currently allowed at a 68% confidence level.

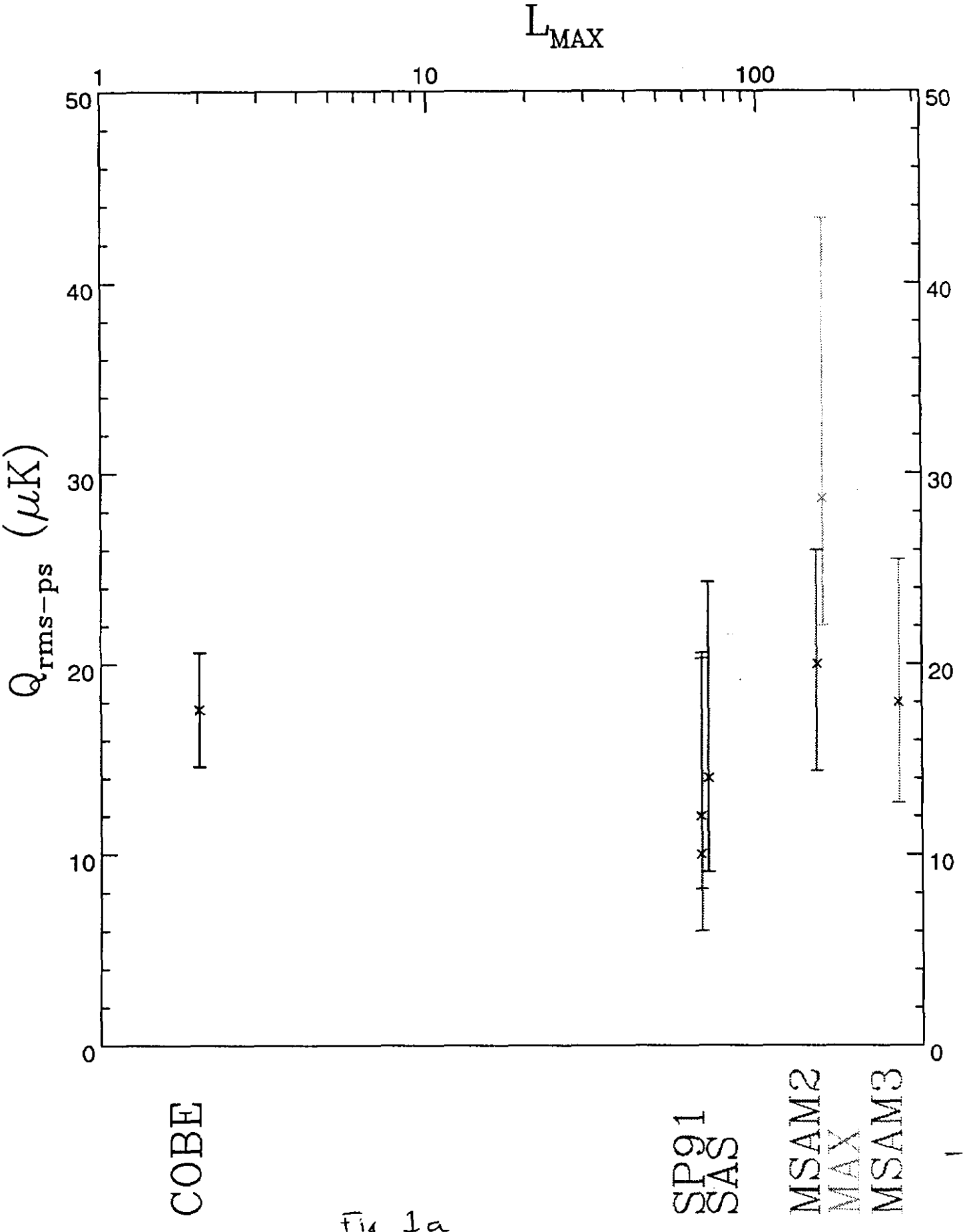
L_{MAX}
1
10
100
50
40
30
20
10
0
Q_{rms-ps} (μK)
COBE
SP91
SAS
MSAM2
MAX
MSAM3

Fig 1a

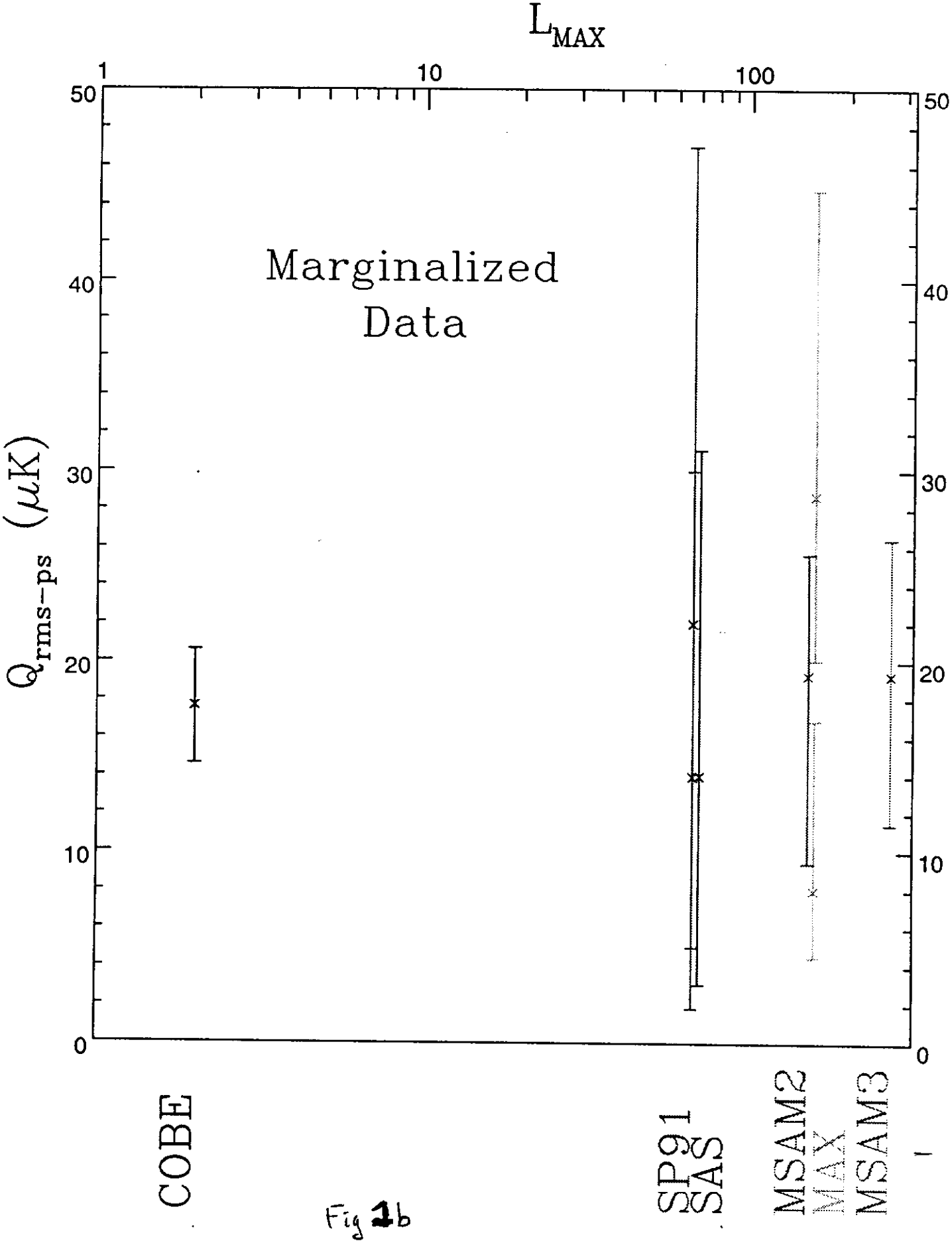
L_{MAX}
1
10
100
50
40
30
20
10
0
Marginalized
Data
Q_{rms-ps} (μK)
COBE
SP91
SAS
MSAM2
MAX
MSAM3

Fig 1b

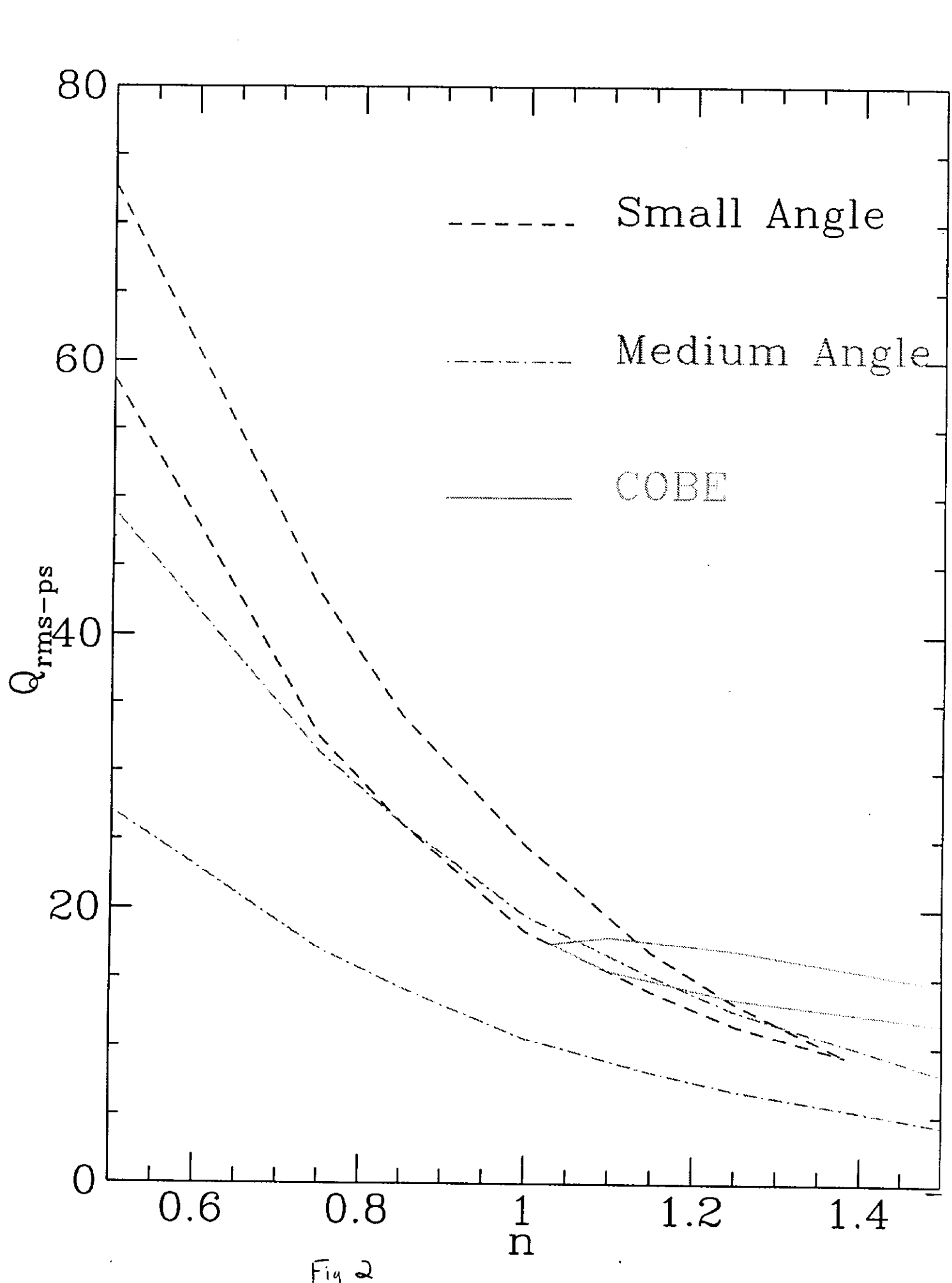
80
60
40
20
0
0.6
0.8
1
1.2
1.4
n
Q_{rms-ps}
Small Angle
Medium Angle
COBE

Fig 2